Design of High-frequency Fast-rise Pulse Modulators for Lifetime Testing of Dielectrics

P. Mathew, M. G. Niasar, and P. Vaessen, *High Voltage Technologies Group, TU Delft, The Netherlands*

***Abstract* — Penetration of power electronics in the grid has produced a new species of stresses, characterised by fast-rising pulsed waveforms with microsecond rise-times repeating at several tens of kilohertz. Analysing their impact on existing and future insulation systems requires pulse modulators, most often with pulse transformers (PT), to perform ageing and breakdown tests. PT design for klystron loads has been studied extensively albeit for either low repetition rates or short pulse durations. However capacitive dielectric loads impose additional complex constraints on optimising leakage (L_σ) and parasitic capacitance (C_d) in order to minimise rise-time (T_r) and overshoot (V_{pk}). Ensuring consistent output pulse shape is crucial since breakdown is sensitive to voltage magnitude. This paper discusses these challenges through the design procedure of a modulator prototype capable of producing bipolar pulses up to 14 kV with rise times < 2 µs at frequencies between 10-50 kHz. Major challenges especially core selection, winding design, PT parasitic optimisation, breakdown detection and failure modes are highlighted. A new PQR equation is derived to model modulators with capacitive loads. Finally, the output pulses are applied across oil-impregnated paper samples to generate statistics on insulation breakdown strength and lifetime at 10 kHz and 50 kHz. Results illustrate a reduction in lifetime and breakdown strength at 50 kHz. This is possibly due to the non-homogenous distribution of dielectric losses within the oil-paper leading to local hotspots and eventual thermal breakdown. Further, a critical field F_c = 21 kV/mm is found below which the slope of the lifeline decreases dramatically thereby indicating a shift in ageing mechanism. Potential reasons for this phenomenon are also discussed.**

***Index Terms*— dielectric ageing, mixed-frequency, high power, pulse modulator, solid-state transformer, oil-paper, pulse transformer, leakage flux, distributed capacitance**

I. INTRODUCTION

THE ongoing energy transition towards a greener future is facilitated by wide-spread application of power electronics in the grid. Increased expertise in high-power and the introduction of silicon carbide has catalysed key technologies such as the solid-state transformers (SST). SSTs are expected to play a vital role in future power systems by offering large energy densities and flexible power flow [1]; although at the cost of severe mixed frequency pulsed stresses experienced by the dielectric insulation of their inverter-fed medium frequency transformers (MFT) [2]. These stresses are characterised by fast-rising pulsed waveforms as in Fig 1.

In contrast to pure sinusoids, the ageing of dielectrics under pulsed stresses is still under investigation. The influence of such waveforms was first observed in an increase of stator winding failures during the widespread application of variable speed drives for motors in the 1980s [3-8]. Kaufhold *et al.* showed that time-to-failure can be predicted by an n_b number of partial discharges (PD) [5]. Yin *et al.* attributed insulation failure to a combinatory effect of partial discharge, dielectric heating and space charge formation [6]. Her work demonstrated that the frequency dependence of insulation lifetime differs under either pulsed or sinuous stress [7]. Montanari *et al.* separated ageing mechanisms above and below the partial discharge inception voltage (PDIV) [8]. Cavallini *et al.* identified pulse magnitude as the dominating ageing factor apart from frequency, rise-time, polarity, and duty cycle [9]. More recent works by Wang *et al.* studied PD characteristics under square waveforms [10] and assessed the impact of rise-time [11], frequency [12], and duty cycle [13] on ageing. Koltunowicz *et al.* also studied the impact of frequency on oil-impregnated paper insulation (OIP) [14-15]. However despite extensive literature, lifetime statistics under pulsed waveforms are not available above a few kHz. Since MFT insulations experience pulses up to 50 kHz, filling this research gap forms the first core motivation of this paper.

Analysing the impact of pulsed waveforms requires pulse modulators to produce quick quasi-rectangular voltages across dielectric samples. An important modulator component is the pulse transformer (PT), the design of which has been studied in-depth such as in klystrons [16-18], treating air pollution [19], and cancer radiation therapy [20-21]. However the capacitive nature of dielectrics need significantly more complex PT design criteria for lifetime tests. The derivation and description of these criteria form the second core motivation of this paper.

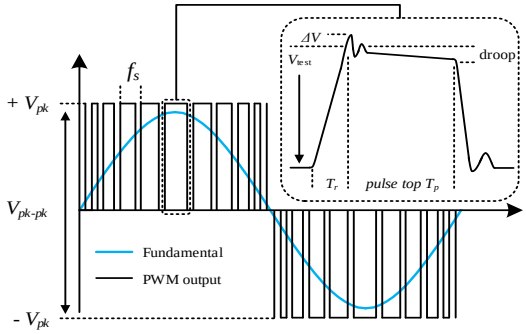

Fig. 1. Typical pulse-width modulated output of a 2-level inverter.

Manuscript received on 12 February 2023. Accepted on 11 July 2023. This research was funded by the Dutch TKI Urban Energy program.
P. Mathew performed his MSc thesis at the HVT Delft group and is now with Hitachi Energy HVDC, Ludvika, Sweden (joemat007@gmail.com)

M. G. Niasar is with the Electrical Sustainable Energy department as an Assistant Professor of the HVT group (m.ghaffarianniasar@tudelft.nl)

P. Vaessen is the HVT Head Professor and Innovation Manager at KEMA Labs Arnhem, The Netherlands (p.t.m.vaessen@tudelft.nl)

Typical values of pulse waveform parameters for 2-level SST inverters compiled from [22-23] are summarised in Table 1.

Table 1. Typical parameter ranges of inverter waveforms.

Parameter	Symbol	Typical range
Peak-to-peak voltage	$V_{pk\text{-}pk}$	500 V – 20 kV
Switching frequency	f_s	5 Hz – 50 kHz
Pulse rise time	T_r	100 ns – 4 µs

Four popular modulator choices are illustrated in Fig 2. Line-type is not picked due to limited pulse shaping [24]. The Marx generator is limited in repetition rate and requires many stages decreasing reliability [25-26]. Series HV-switches are suitable and have been used extensively for dielectric tests in literature [27-28]. However the implementation of this topology requires:

- A high-voltage DC source which can be quite expensive
- High-voltage switches that can be expensive to procure
- Series inductance to limit current after dielectric breakdown

The LV-switch with PT topology was selected instead. This setup can be sourced at 230 V, implemented with inexpensive switches, produce both uni/bi-polar pulses, and also has a short-circuit limitation from the inductance of the pulse transformer.

Table 2. Comparison of modulator topologies.

Topology	Advantage	Disadvantage
Line-type	Relatively compact	Limited shape control
Series HV-switch	Simple design	↑ Cost (source, switch)
Marx generator	Sourced at LV	↑ N_{stages} = ↓ reliability
LV-switch + PT	Flexible control	Transformer parasitics

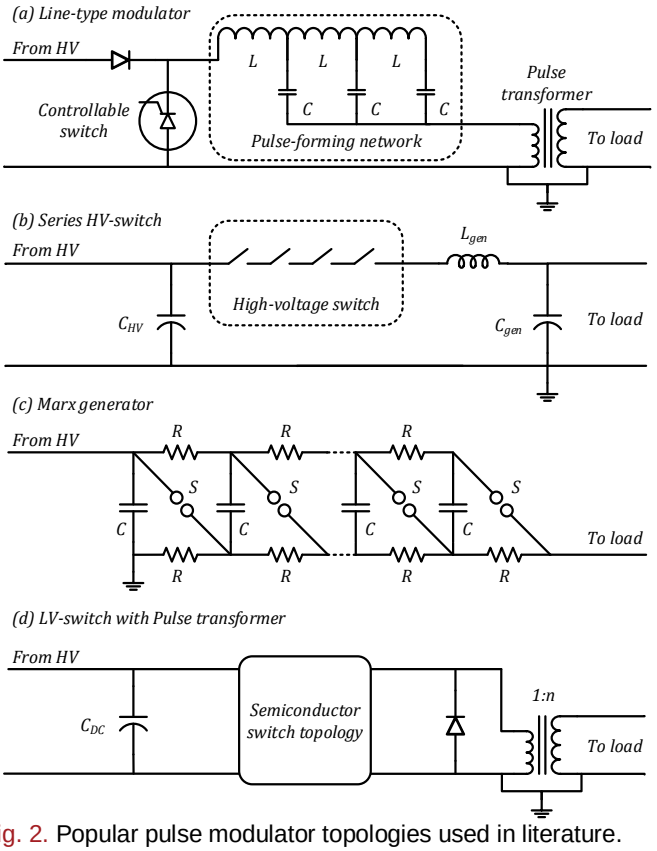

Fig. 2. Popular pulse modulator topologies used in literature.

II. MODULATOR MODEL

Owing to their diverse application set, pulse modulators have been modelled extensively to accurately predict the output waveform at a certain operating point. The standard IEEE 390 model [29] is shown in Fig 3 (a) with the following elements,

- Ideal transformer of ratio n
- Ideal pulse generator U_g
- Output load impedance Z_{load}
- Winding resistances R_{11}-R_{21}
- Leakage inductances L_{11}-L_{21}
- Distributed winding self-capacitances C_1-C_2
- Inter-winding capacitance C_{12}
- Core-loss resistance R_c and magnetizing inductance L_m

In the time-domain, a pulse can be divided into three unique portions viz. leading edge T1, pulse top T2, trailing edge T3. The dynamics during these durations can be studied separately as shown in Fig 3 (b) (remains applicable to the nanosecond scale [16]). In T1, shunt R_c and L_m is removed due to negligible core excitation in short rise-times. In T2, series L_σ and shunt C_d is neglected since only low-frequency components are present. Parameters of interest are rise-time (T_r) and overshoot (ΔV) in T1 and pulse droop in T2. Since tests will be performed with bipolar pulses, T3 parameters such as settling time will have no impact. In the next section a relation from T_r and ΔV to PT parasitics L_σ and C_d is derived for resistive and capacitive loads.

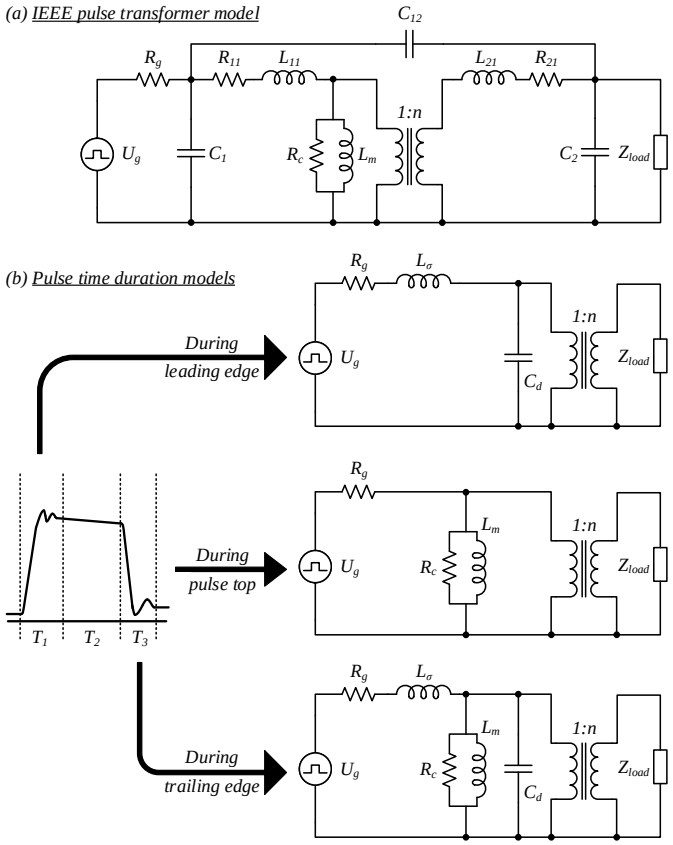

Fig. 3. (a) IEEE 390 standard equivalent circuit for a pulse transformer (generic load) and (b) splitting into three separate circuits for modelling characteristics during each pulse duration.

A. For Resistive loads

The equations for resistive-load pulse transformers, as shown in Fig 4 (a), were first derived by W.H. Bostick of the MIT Radiation Laboratory in 1948 [30]. This combined with [16] linked the transformer leakage flux L_σ and parasitic capacitance C_d with the parameters rise-time T_r and peak overshoot ΔV as:

$$2\,R_{load}\cdot\sigma = \sqrt{\frac{L_\sigma}{C_d}} \quad (1) \qquad T_r = 2\pi\cdot T_{10\%-90\%}\sqrt{L_\sigma C_d} \quad (2)$$

where σ is the damping coefficient and $T_{10\%-90\%}$ is the time taken for voltage magnitude to rise from 10% to 90%. The key observation was that rise-time reduction requires minimising parasitic product $L_\sigma C_d$ while peak overshoot reduction requires minimising parasitic ratio $\frac{L_\sigma}{C_d}$ causing a compromise. Bortis *et al.* showed the product depends on physical design while the ratio depends on the choice of transformer inter-connections [16].

B. For Capacitive loads

Unlike the above equations, pulse modulators for dielectric testing will instead see a load insulation sample modelled as a capacitance. However this C_{load} would be added to parasitic C_d resulting in zero damping (high overshoots) and longer rise-times:

$$\sigma \propto \frac{1}{R_{load}}\sqrt{\frac{L_\sigma}{(C_d + C_{load})}} \xrightarrow{R=0} 0 \quad (3) \quad ; \quad T_r \propto \sqrt{L_\sigma(C_d + C_{load})} \quad (4)$$

The solution utilised in this paper is to add the test elements R_t and C_t as shown in Fig 4 (b). The inclusion of R_t decouples transformer-load dynamics, while the R_t C_t combination filters the output pulse waveform with a cut-off frequency defined as:

$$F_c = \frac{1}{2\pi\cdot R_t C_t} \quad (5)$$

Since C_{load} depends on both electrode arrangement and insulation sample thickness and permittivity, this pulse tuning capability is necessary in order to ensure consistent waveform shape throughout all tests, considering breakdown is most sensitive to peak voltage.

Further, R_t limits steady-state short-circuit current through the modulator after dielectric breakdown occurs, while the transformer inductance slows down the dynamic current-rise providing a sufficient time window to disconnect the modulator from the load.

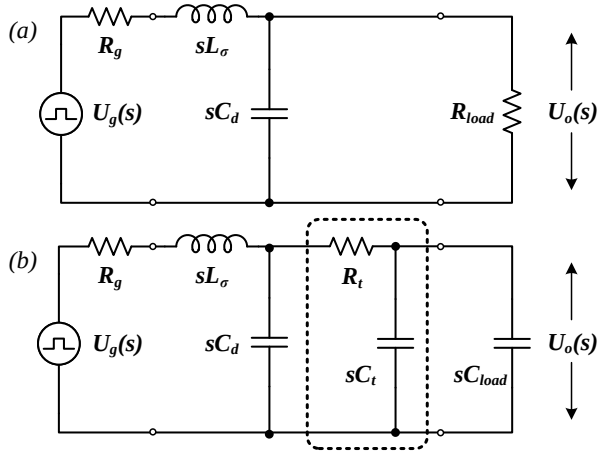

Fig. 4. Equivalent circuit with (a) resistive (b) capacitive loads.

The addition of R_t and C_t thus results in a third-order circuit. After simplifications, the output voltage can be expressed as:

$$U_o(s) = \frac{U_g}{sL_\sigma C_d R_t C_{eq}} \times \frac{1 + sR_t C_{eq}}{s^3 + s^2\left(\frac{1}{R_t C_{eq}} + \frac{1}{R_t C_d}\right) + s\left(\frac{1}{L_\sigma C_d}\right) + \left(\frac{1}{L_\sigma C_d R_t C_{eq}}\right)} \quad (6)$$

Setting $C_{eq} = C_t + C_{load}$ and $R_g \approx 0$, the equation reduces to:

$$U_o(s) = \frac{U_g}{s} \times PQ \times \frac{1}{s^3 + s^2 R + s\,P + P\,Q} \quad (7)$$

$$P = \frac{1}{L_\sigma C_d} \qquad Q = \frac{1}{R_t C_{eq}} \qquad R = \frac{1}{R_t}\left(\frac{1}{C_{eq}} + \frac{1}{C_d}\right) \quad (8)$$

where,
Parasitics parameter (P) represents transformer dynamics
Quality parameter (Q) represents dynamics of the R_t C_{eq} filter
Relational parameter (R) represents coupling between P and Q

This PQR equation (7) can be solved for $u_o(t)$ with varied values of L_σ C_d R_t C_t from a default L_σ = 250µH C_d = 200pF R_t = 10kΩ C_t = 60pF C_{load} = 50pF to illustrate the impact of each element.

From Fig 5 (a), achieving faster rise-times and lower overshoots clearly requires minimisation in transformer parasitics. But it also shows that even unrealistically low values of L_σ C_d produce an atmost critically damped response, further demonstrating the limitations when designing transformers for capacitive loads.

On the other hand, the advantageous effect of R_t Ct is illustrated in Fig 5 (b) where an increase of either results in lower cut-off frequency and lower overshoot. It is thus vital to have these test elements for tuning output pulse shape for dielectric tests with different electrode arrangements and insulation permittivities.

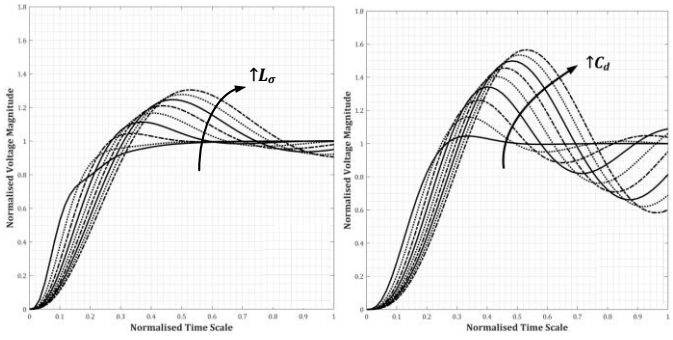

Fig. 5. (a). Effect of transformer parasitics on output pulse-rise.

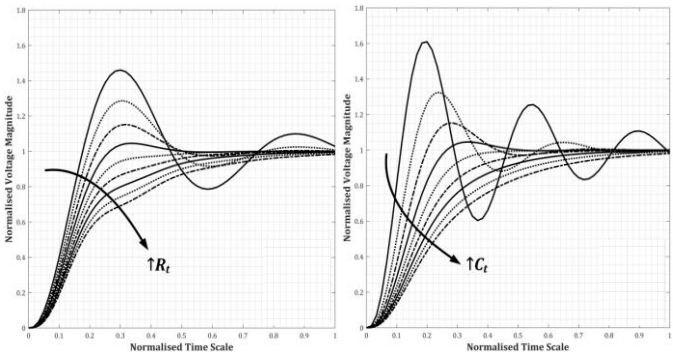

Fig. 5. (b). Effect of modulator tuning elements on pulse-rise.

III. MODULATOR PROTOTYPE

This section describes the design of a modulator with desired specifications in Table 3. Input is 230 V fed from AC mains. An output of 14 $kV_{pk\text{-}pk}$ is required for testing samples. Load capacitance C_{load} = 30 pF is calculated for a single-layer OIP sample of thickness 150 µm and electrode diameter of 2.54 mm. Turns ratio of n = 50 was chosen to reduce primary turns. Pulse frequency should be variable from 10 to 50 kHz for studying impact of frequency on dielectric lifetime. Output should have minimal overshoot since sample breakdown is mostly sensitive to peak voltage magnitude. The modulator should be capable of producing sustained pulses over several hours for lifetime tests without any waveform change. During breakdown tests, a ramp of 1 kV/s is to be applied. There should exist a reliable method for controlling this rise. Finally, the modulator should disconnect within a short time-frame to reduce electrode breakdown marks.

Table 3. Desired pulse modulator specifications (refer Fig 7).

Parameter	Symbol	Usual range
DC link voltage	V_{in}	230 V
Maximum test voltage	V_{test}	14 $kV_{pk\text{-}pk}$
Transformer turns ratio	n	1:50
Pulse repetition rate	f_s	10 – 50 kHz
Pulse overshoot	ΔV	< 1 % V_{test}
Pulse rise (0-100%)	T_r	< 20 % $(2f_s)^{-1}$
Load capacitance	C_{load}	30 pF

Unlike sine-wave transformers, pulse transformers transmit a bandwidth of frequencies [f_{lower} f_{upper}]. Frequency spectrum of a sample 50 kHz pulse is analysed in Fig 6. The f_{lower} is limited by the core saturation criteria while f_{upper} is limited by parasitics L_σ and C_d of winding design. The fundamental dominates but there also exists a significant higher frequency content in the range of several hundreds of kHz corresponding to rise-times. The pulse waveform parameters are defined as shown in Fig 7.

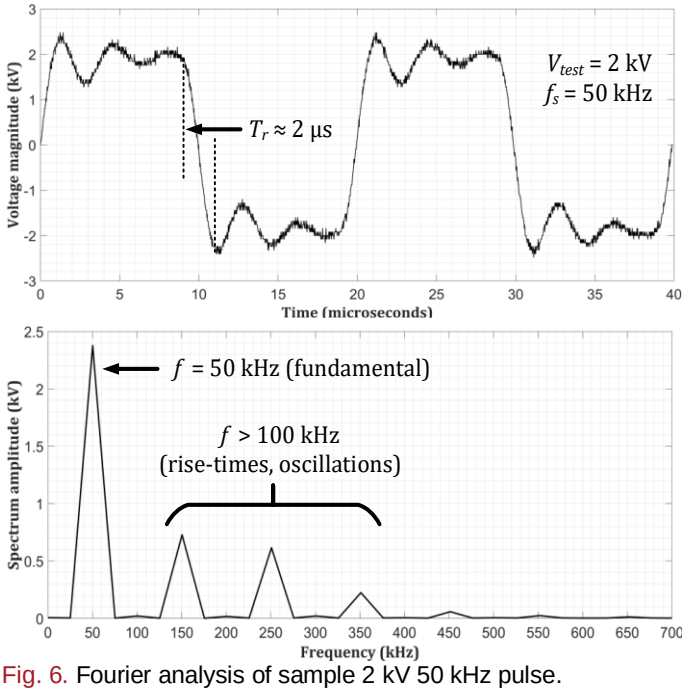

Fig. 6. Fourier analysis of sample 2 kV 50 kHz pulse.

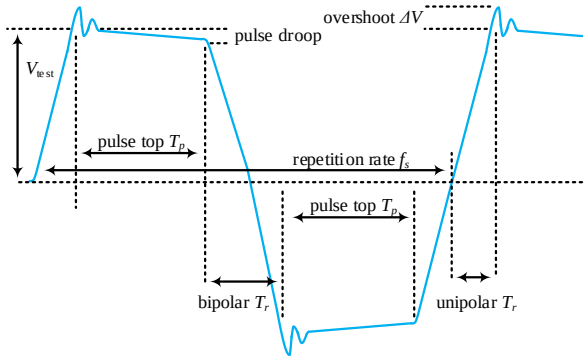

Fig. 7. Definitions of bipolar pulse waveform parameters.

A. Magnetic Core

The magnetic core tightly bundles the flux lines within itself, increases magnetic field density, and improves linking between the windings. Commonly used materials include iron-based alloys (high B_{sat} but high losses) and soft ferrites (low B_{sat} but low losses). The unipolar PT in [6] used an amorphous iron-based magnetic alloy from Metglas USA with a B_{sat} = 1.6 T. However such cores are expensive and highly lossy for faster sustained repetition rates. Instead, an N87 MnZn ferrite U-core from TDK was selected with specifications detailed in Table 4.

Table 4. N87 MnZn TDK magnetic core parameters.

Parameter	Symbol	Usual range
Saturation flux at 25°C	B_{sat}	500 mT
Cross-sectional area	A_e	840 mm^2

This selection of a ferrite core now imposes limitations on the saturation prevention criteria. The maximum flux swing ($\Delta B = 2B_{max}$) under a bipolar excitation depends on the volt-per-turn $\frac{V_{max}}{n_1}$, the pulse duration T_p and core cross-section expressed as:

$$B_{max} = \frac{V_{max} \cdot T_p}{2 \cdot n_1 \cdot A_e} \quad (9)$$

An operating B_{max} = 400 mT was selected considering the increase in temperature (decrease in B_{sat}) due to core losses. The required primary turns to prevent core saturation at 10 kHz is:

$$\Rightarrow \; n_1^{min} = \frac{230\,V \cdot 50\,\mu s}{2 \cdot 400\,mT \cdot 840\,mm^2} \approx 17\,turns$$

However this would lead to drastically high L_σ values, high overshoots, and slow rise-times. To reduce the L_σ klystron modulators commonly have a single turn primary (n_p = 1), but this option is only possible when producing pulses of short duration ≈ 5 µs [16] or at low repetition rates [31-32]. An 8-core structure (Fig 8) is used instead for a four-fold increase in cross-section, thereby reducing the criteria to $\boldsymbol{n_p = 4}$. This design also reduces the effective reluctance improving magnetic linkage.

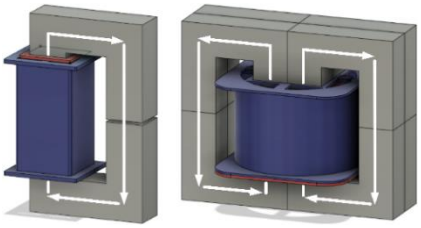

Fig. 8. Comparison of 2-core (left) and 8-core (right) geometries.

B. Winding Design

Designing an optimal winding involves balancing sufficient clearances (which cause flashovers) and transformer parasitics (which affect pulse performance). These trade-offs are further strained due to limited window size of the chosen N87 core. The geometrical parameters of the PT design are illustrated in Fig 9.

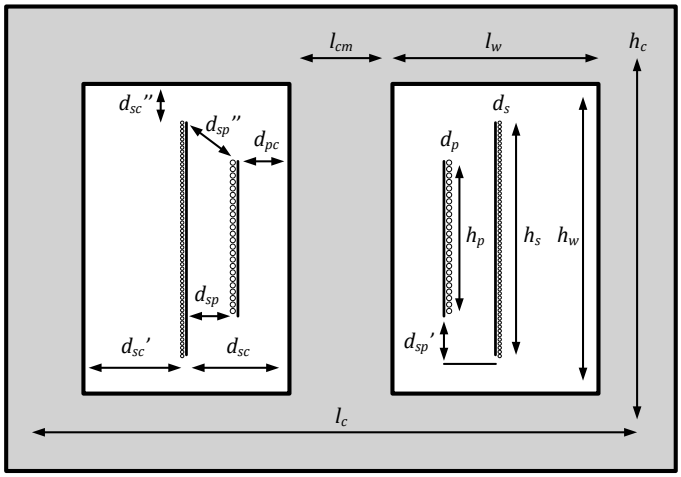

Fig. 9. Geometrical parameters of PT design (not to scale).

Primary winding parameters

Foil windings are ideal for reducing leakage ($h_p = h_s$) but their construction can be quite difficult for $n_p > 1$. Enameled wire can be used instead despite relatively larger leakage. This L_σ can then be reduced by spreading the turns across h_p but this also reduces d_{sp}'' isolation leading to severe HV-LV flashovers as in Fig 10. As a trade-off, silicon insulated (thickness 3 mm) wire was selected.

Primary and secondary currents of the PT can be calculated as:

$$I_s = 4 \cdot \frac{C_{load} \cdot V_{test}}{T_r} = 4 \cdot \frac{30\,pF \cdot 7\,kV_{pk}}{4\,\mu s} \approx 210\,mA \quad (10)$$

$$I_p = n \cdot I_s = 50 \cdot 210\,mA \approx 10.5\,A \quad (11)$$

Hence d_p = 2 mm is selected for a 3 A/mm^2 current density. The final measured height of the primary winding is h_p = 35 mm and the d_{pc} = 3 mm is now the thickness of the wire silicon insulation.

Secondary energisation induces a potential onto the core causing LV-core discharges leading to damages on the LV structure as shown in Fig 11. This potential was estimated with finite element analysis (FEA) and measured with an electrostatic voltmeter to be 0.3 times the V_{test} magnitude. The core is thus grounded and d_{pc} kept as short as possible to provide flexibility for other trade-offs.

Fig. 10. Flashover at V_{test} = 17 kV$_{pk\text{-}pk}$ between highest potential of HV to LV winding due to an insufficient d_{sp}'' isolation distance.

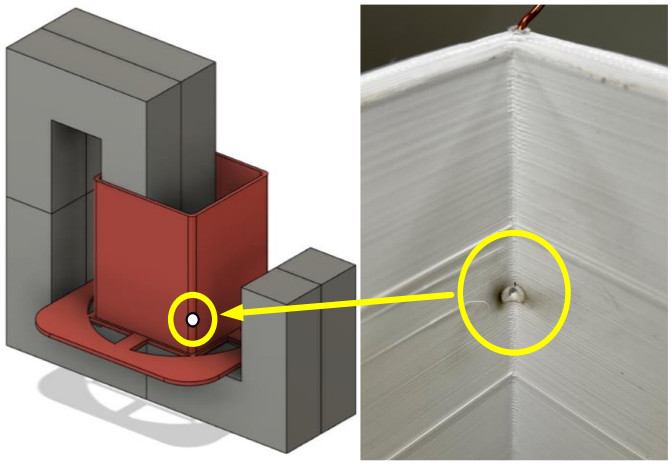

Fig. 11. Structure damage due to repeated LV-core discharges.

Improper grounding can cause discharges between core pieces, only diagnosed with auditory feedback. Each core interface was then coated with a 1:1 (catalyst:base) paste mixture of TFC Silicone Rubber Type 3 and conductive carbon black. Larger paste volumes can decrease inductance and cause pulse droop.

Secondary winding parameters

Enamled wire of d_s = 0.35 mm is selected to construct a 200 turn secondary HV winding of height h_s = 70 mm. This is made in a single-layer so as to reduce C_d parasitic. The transformer is 3D modelled for FEA as illustrated in Fig 12. Secondary voltage V_{test} is implemented as a gradient along the HV winding length.

The vertical position of the primary winding (d_{sp}') influences the HV-LV field stresses and is hence set to 0 mm to limit the average field strength to 500 V/mm as in Fig 13. The largest possible vertical clearance between the highest potential of the HV winding to the grounded core is d_{sc}'' = 20 mm for this core.

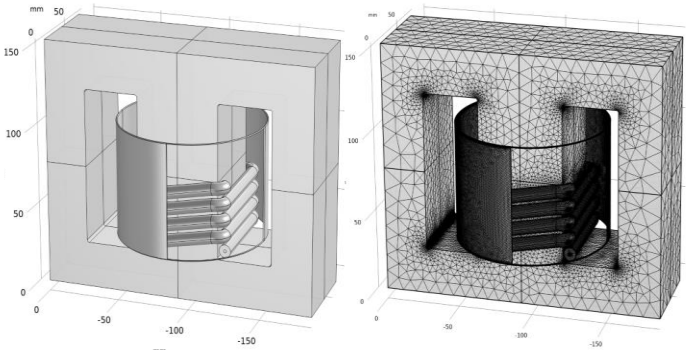

Fig. 12. 3D FEA model and mesh of prototype pulse transformer.

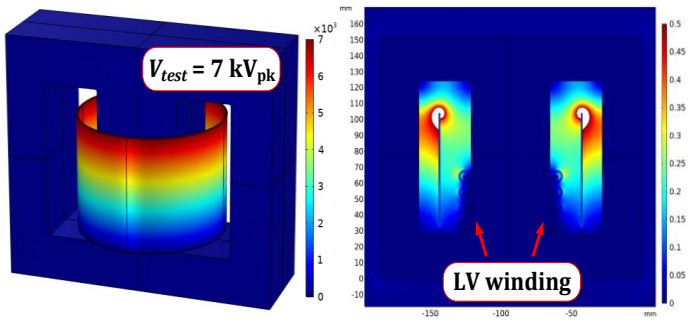

Fig. 13. HV potential distribution (left: 0 – 7 kV$_{pk}$) and E-field magnitudes inside PT window from FEA (right: 0 – 0.5 kV/mm).

It can be seen in Fig 13 that the highest field stresses occur at the top of the HV winding. This can be studied with an xy 2D cut plane slicing the transformer model as shown in Fig 14. The curvature of the secondary results in two critical points *viz.* at the d_{sc}' inside the transformer and at an external distance d_{sc}''' (Fig 14). Since an increase in either of these clearances reduces the other, an optimal balance is found at d_{sc}' = 12.5 mm and d_{sc}''' = 11.5 mm through FEA. The average field strength in this area also satisfies the 500 V/mm limit. The peak stresses here are improved by applying insulating grease on the winding. It should also be noted that liquids are unsuitable as an alternative medium due to non-unity permittivities ($\varepsilon_r \neq 1$) multiplying with C_d parasitic. SF_6 can offer desirable properties but is not considered due to negative environmental impact, and high-pressure gases will require expensive gas-tight enclosures.

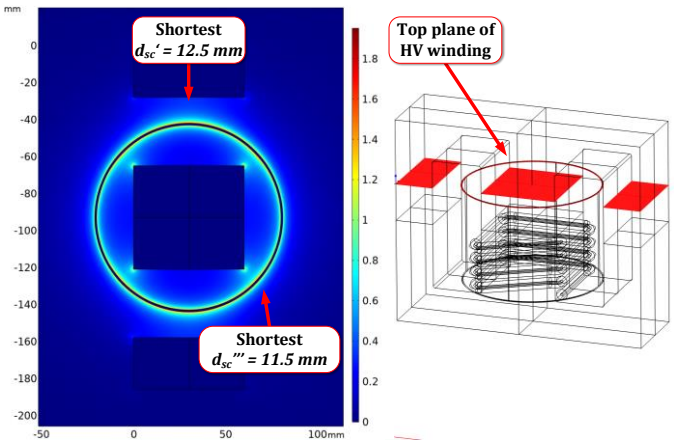

Fig. 14. Obtained E-field magnitudes (left: 0 – 1.9 kV/mm) and studied 2D xy cut plane at the top of HV winding (right: red).

Parasitic evaluation

The final PT prototype is shown in Fig 15. The silicon-insulated LV winding is contained inside the HV secondary. These were designed in CAD and 3D printed in polylactic acid (PLA). The core is uniformly grounded and held together in a plexiglass frame. Measured PT parasitics are L_σ = 730 µH and C_d = 25 pF.

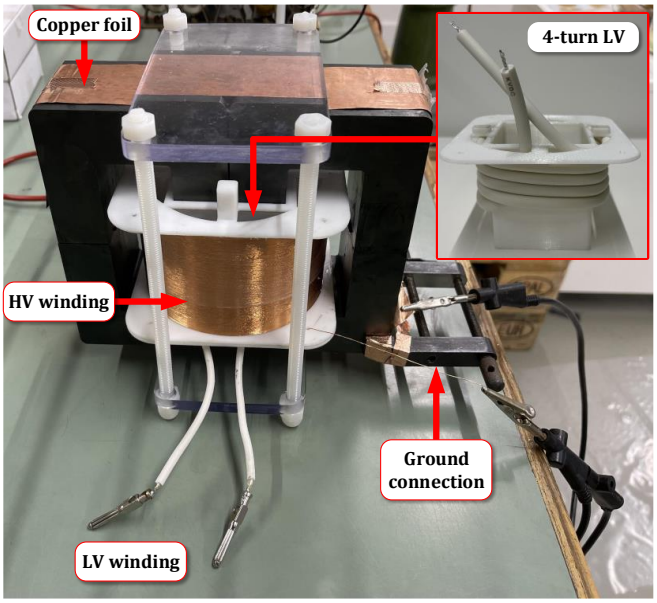

Fig. 15. Final PT prototype (note that LV is shown inverted here).

Table 5. Summary of final PT geometry values (refer Fig 9).

Primary LV	Secondary HV	Core
n_p = 4 turns	n_s = 200 turns	N_c = 8 core pieces
d_p = 2 mm stranded	d_s = 0.35 mm solid	h_c = 152 mm
h_p = 35 mm	h_s = 70 mm	l_c = 186 mm
d_{pc} = 3 mm	d_{sc} = 22.5 mm	l_{cm} = 20 mm
d_{sp} = 10 mm	d_{sc}' = 12.5 mm	h_w = 96 mm
d_{sp}' = 0 mm	d_{sc}'' = 20 mm	l_w = 37 mm
d_{sp}'' = 45 mm	d_{sc}''' = 11.5 mm	A_e = 3360 mm^2

D. Variable Test Elements

Test elements include a series R_t and a parallel C_t which can tune output pulse shape and ensure consistency across tests.

R_t is implemented as a bank of three series sets of five parallel high-power resistors as shown in Fig 16. Since values above R_{t_max} = 20 kΩ overdamp the output pulse as in Fig 17 hence an R_t = 17.75 kΩ is implemented with combinations of 20 kΩ and 50 kΩ. This reduces the power dissipation per resistor ensuring stable temperatures (and resistance) during long ageing tests.

C_t is implemented as a high voltage capacitor connected in parallel to the test sample as in Fig 16. The disk diameter is 20 cm and the distance between disks (d) can be altered with a rotational handle. Smaller d increases C_t and thereby the pulse damping, which is important since R_t alone cannot be used to tune output wave shape (R_{t_max} criterion). Typical C_t magnitudes between tests at 10 – 50 kHz ranged between 50 – 150 pF.

Impact of tuning R_t C_t on the pulse shape is illustrated in Fig 18.

Fig. 16. Left: Resistance bank (R_t) Right: HV disk capacitor (C_t).

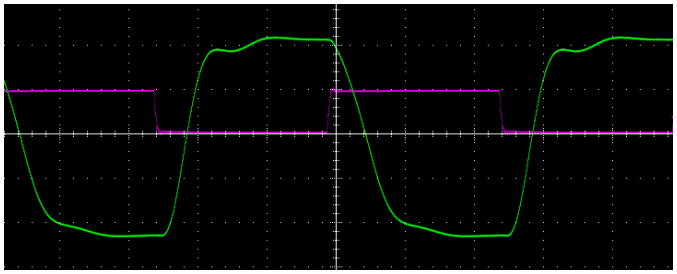

Fig. 17. Pulse shape (green) deformation above R_{t_max} = 20 kΩ.

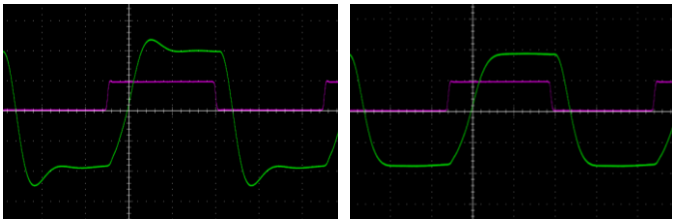

Fig. 18. Pulse shape without (left) and with (right) R_t C_t elements.

D. Breakdown Detection

In the event of insulation breakdown, the modulator must automatically disconnect the supply in a few milliseconds. In the absence of this function a conducting arc will gradually burn the oil-paper sample and cause electrode deformation (Fig 19). To prevent this, an analog circuit was designed in the ESE Lab, TU Delft to detect dielectric breakdown. Since $\frac{dV}{dt}$ of output waveform is high it cannot be used as a trigger parameter. Instead, the detector is connected in series to and measures over-current through the test sample. Further, the current flowing through the capacitive sample increases for higher frequencies, requiring adjustment of over-current threshold for breakdown detection. If the detector is made over-sensitive it would disconnect before dielectric breakdown, statistically neglecting healthy samples. If under-sensitive, breakdown arcs are longer leading to carbonisation and electrode deformation. Few reference test samples were checked after breakdown under an Olympus SZH-ILLD microscope. The effect of pulse frequency and detection sensitivity is illustrated in Fig 20. The burn mark was observed to be sharper at 50 kHz than at 10 kHz.

Fig. 19. Electrode breakdown marks requiring sand-polishing.

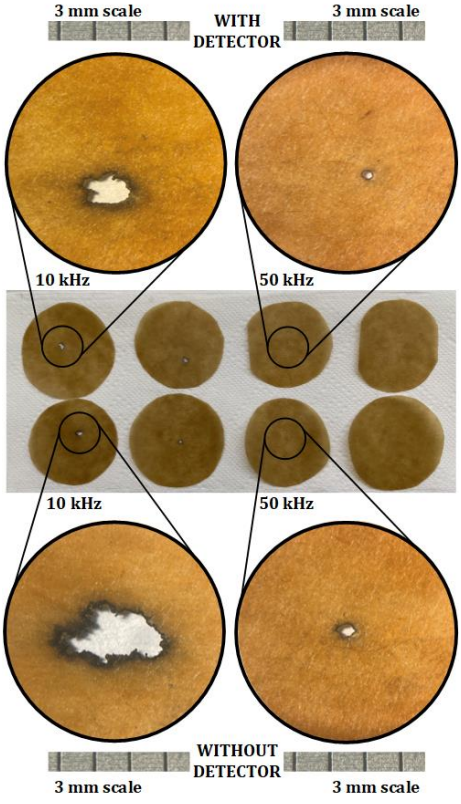

Fig. 20. Effect of sensitivity-frequency on breakdown mark.

E. Prototype Summary

An overview of the built prototype pulse modulator is provided in Fig 21. The system operates in the following three stages:

- The source 230 V_{AC} mains is isolated through a transformer and recitified to a smooth DC with a thyristor bridge.
- The bridge powers an H-bridge pulse generator PCB which produces 650 $V_{pk\text{-}pk}$ bipolar pulses controlled by an Arduino.
- The low voltage pulses are stepped up through the designed 1:50 pulse transformer and tuned by test elements R_t and C_t before being applied across the oil-immersed test sample.

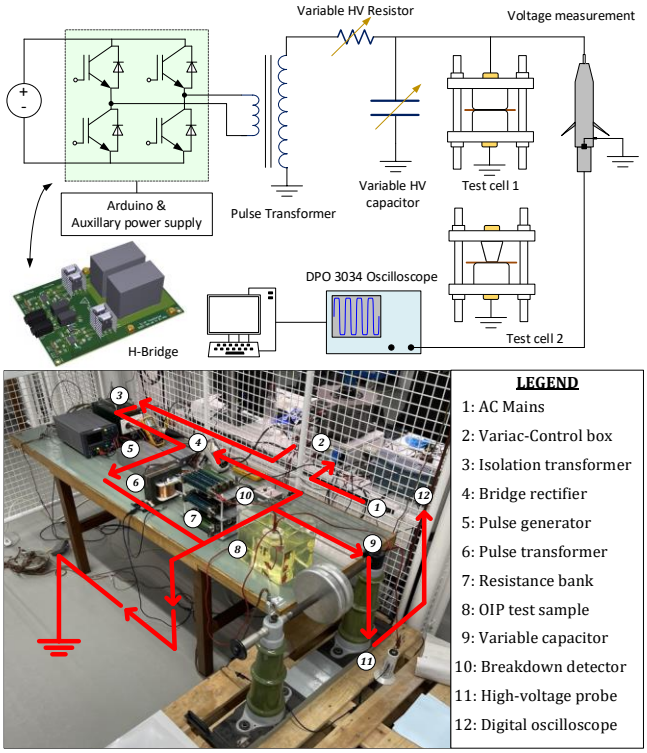

Fig. 21. Overview of modulator prototype for dielectric testing.

Output pulse waveform is analysed in Fig 22. Measured rise-time $\boldsymbol{T_r = 1.84\ \mu s}$ (Fig 22) satisfies the $T_r < 0.2T_p$ criteria in Table 3. Measured pulse tops were $\boldsymbol{T_p = 6.32\ \mu s}$ at 50 kHz and $\boldsymbol{T_p = 46.32\ \mu s}$ at 10 kHz. Pulse overshoot was critically damped ($\Delta V \approx 0$) for all tests to study the impact of pulse frequency. Duty cycle was set to 50 %. In the next section, these pulses will be applied in tests.

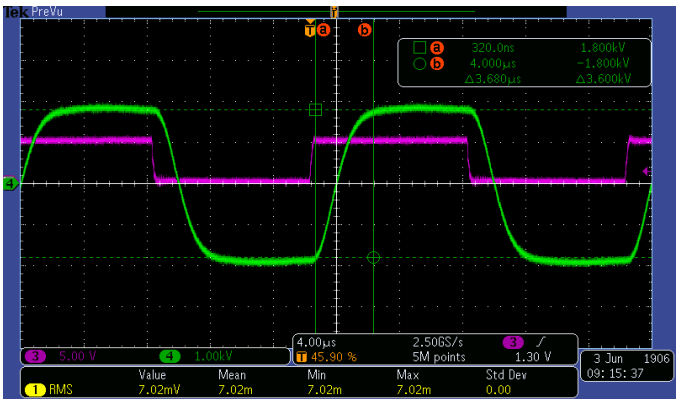

Fig. 22. Measurement of pulse parameters at 50 kHz.

IV. DIELECTRIC TESTING

This section applies the developed pulse modulator prototype in performing dielectric tests. OIP samples of average thickness 150 µm are cut and impregnated inside a vacuum oven as shown in Fig 23. Samples are kept under oil, transferred to the test setup, and stored later for breakdown pattern analysis [33].

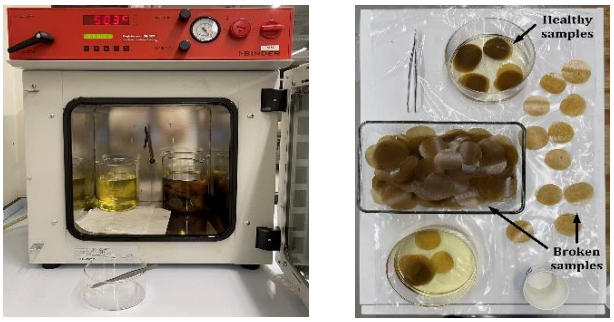

Fig. 23. Preparation workflow of OIP samples for pulsed tests.

A. Breakdown strength

To determine the breakdown strength of insulation samples with cylindrical and conical electrodes, pulsed waveforms at 50 kHz ramping at 1 kV_{pk}/s were applied. The cumulative failure probability *F(E)* is linearised across field magnitudes. This is expressed according to the Weibull probability model:

$$F(E) = 1 - e^{-\left(\frac{E_{break}}{\alpha}\right)^{\beta}} \quad (12)$$

The shape parameter β in Table 5 is the slope of the resultant line while the scale parameter α represents the E_{break} at an *F(E)* = 63.2 %. Plotting *F(E)* against breakdown strengths produces Fig 24. The cylindrical electrode shown in Fig 19 applies field uniformly across a larger area, thereby lowering breakdown strength (shifted left), and was hence selected for lifetime tests.

Table 6. Obtained Weibull distribution parameters.

Parameter	β	α
Conical electrode	32.3	18.1 kV/mm
Cylindrical electrode	31.3	17.8 kV/mm

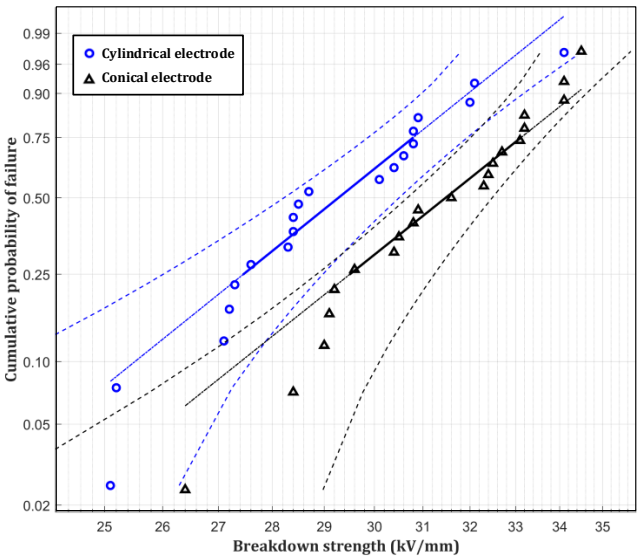

Fig. 24. Breakdown distribution for cylindrical/conical electrodes.

B. Accelerated ageing

To perform lifetime tests, six E-field values were chosen with the highest value lower than the lowest breakdown strength $E_{break} \approx 25$ kV/mm (Fig 25). A total of 292 tests were performed with 20-41 tests at each field. R_t temperature was kept < 50°C with a fan and measured at intervals. Electrodes were polished after breakdowns. Failure time is plotted logarithimically in Fig 25. Median lifetimes (blue points) are connected with a best-fit line to obtain lifelines at 10 kHz and 50 kHz. The remaining lifetime can then be expressed as an inverse power law model:

$$T_{life} = k\left(\frac{E}{E_0}\right)^{-n} \quad (13)$$

Constant *k* has a unit of time (seconds) while E_0 has a unit of field strength (V/mm). Slope *n* indicates sensitivity of lifetime to field variation. Obtained values are summarised in Table 6.

Table 7. Obtained lifetime curve parameters.

Parameter	*n*	*k*
10 kHz (above transition)	9.5	1.7×10^{15} s
50 kHz (above transition)	6.9	2.1×10^{10} s
50 kHz (below transition)	37.5	3.6×10^{50} s

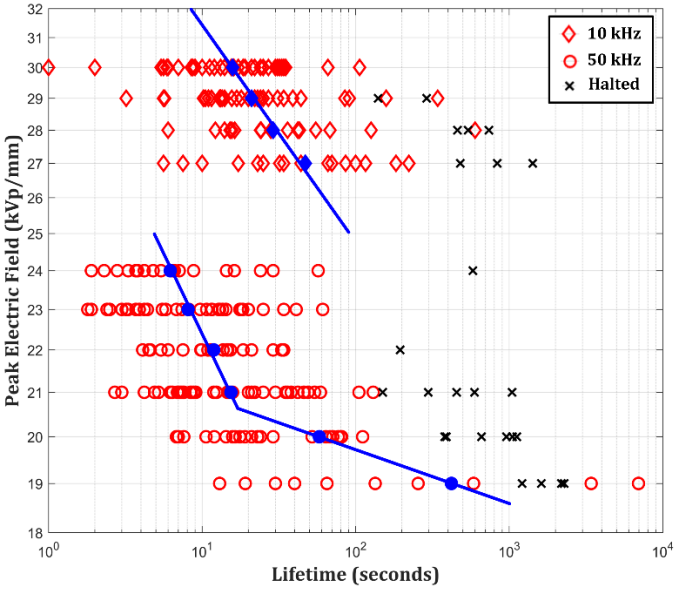

Fig. 25. Obtained lifelines at 10 kHz (red diamonds) and 50 kHz (red circles) by connecting median points (blue points). Halted experiments (black crosses) are included in median calculation.

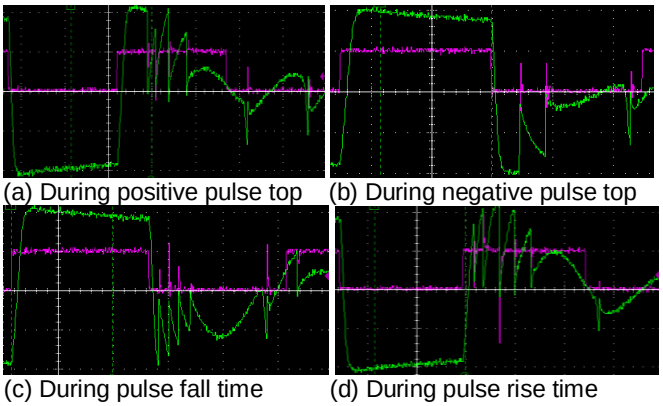

(a) During positive pulse top (b) During negative pulse top

(c) During pulse fall time (d) During pulse rise time

Fig. 26. Observed breakdown instants during dielectric testing.

C. Analysis of ageing results

Trends observed from Fig 25 can be divided into two aspects.

Frequency impact – dielectric lifetime and breakdown strength at 50 kHz is reduced when compared to 10 kHz. This aligns well with previous observations in literature between 50 Hz and 1500 Hz [33]. One potential cause is the increased dielectric losses leading to excessive heating in the insulation when stressed with higher frequency components [34]. However the OIP sample is immersed in oil, an effective thermal conductor with low loss tangent. Hence it is unlikely that the temperature of the test object would increase. The failure could then be due to the non-homogenous nature of the oil-paper itself. This would result in an irregular temperature gradient within the dielectric with local hotspots which eventually cause local (and over time, global) failure of the insulation. Tests at higher frequency produce larger capacitive losses, bring about earlier thermal breakdowns, and hence have shorter failure times.

Electric field impact – dielectric lifeline at 50 kHz seems to "slow down" below a certain critical field $F_c \approx 21$ kV/mm. A similar bend has been mentioned in two literature, amongst others:

Firstly, Yin *et al.* indicated that the dielectric losses in magnet wire dramatically increase above the partial discharge inception voltage level (PDIV) [7]. These discharges produce heat within the dielectric leading to higher leakage currents and losses. This PDIV level has been shown to depend on pulse parameters [35].

Secondly, Crine linked a space charge injection in polyethylene (PE) above a critical field to an accelerated dieletric ageing regime [36-37]. His work predicted a transition at F_c = 18-20 kV/mm at which any injected charges that have energies greater than the polymer cohesion energy can break weaker van der Waals bonds and speed up the insulation ageing process [38].

Two alternate hypotheses for this bend are also explored below:

- Field enhancement in oil-filled cavities between individual paper fibres can exceed local PDIV and accelerate ageing.
- Field enhancement at electrode edges exceeding local oil PDIV can accelerate ageing due to discharges. However the breakdown burn marks of tested samples were always seen to be at the centre, hence ruling out this explanation.

Although the above correlations sound promising, they must be explored further with extensive statistics specifically with oil-paper insulations. The modulator design presented in this paper provides confidence in performing future research to fill this gap. It should also be noted that this phenomenon could not be observed at lower frequencies since the field strengths required for breakdown are far larger than the observed F_c value. High frequencies allow us to study low-field dielectric dynamics.

Finally, breakdown instants are analysed in Fig 26. Statistics from 20 tests given (Table 8) show that most failures occur at the pulse top. It was seen that failures during pulse rise or fall usually occur at the end of the transition near maximum voltage.

Table 8. Statistics of breakdown instants of 20 tests at 10 kHz.

Breakdown instant	Breakdowns	Percentage
Pulse tops	14	70 %
Pulse rise or fall	6	30 %

V. CONCLUSIONS

This paper illustrates the complexities involved in developing pulse modulators for dielectric testing. A new PQR equation is derived to model such systems, since existing literature cannot be applied to capacitor loads. The design procedure for a prototype modulator is described; navigating challenges such as tight core saturation criteria, optimisation of transformer parasitics and failure modes. Test elements R_t Ct allow pulse shaping for consistent testing. Future work is aimed at applying the PQR equation to different modulator prototypes towards building a single comprehensive design optimisation model.

Breakdown and ageing tests are performed on OIP samples at 10 kHz and 50 kHz with pulses of T_r = 1.84 µs. A significant reduction is seen in lifetimes at 50 kHz. This is potentially due to the non-homogenous distribution of dielectric losses leading to local hotspots in the insulation which eventually cause thermal breakdown. Increased losses at higher frequencies hence lead to shorter lifetimes. A critical field level F_c = 21 kV/mm is found below which ageing is slowed, possibly the transition into the non-PD regime of oil-filled cavities between paper fibres. Future research is aimed at generating a lifeline at 30 kHz and identify the F_c to understand if its value is an inherent property of the material itself or instead depends on pulse frequency.

REFERENCES

[1] J. W. Kolar & G. Ortiz "Solid-State-Transformers: Key Components of Future Traction and Smart Grid Systems," 2014.

[2] M. Ghassemi, "Accelerated insulation aging due to fast, repetitive voltages: A review identifying challenges and future research needs," in IEEE Transactions on Dielectrics and Electrical Insulation, vol. 26, no. 5, pp. 1558-1568, Oct. 2019, doi: 10.1109/TDEI.2019.008176.

[3] J. A. Oliver and G. C. Stone "Implications for the application of adjustable speed drive electronics to motor stator winding insulation," in IEEE Electrical Insulation Magazine, vol. 11, no. 4, pp. 32-36, July-Aug. 1995, doi: 10.1109/57.400762.

[4] J. P. Bellomo, P. Castelan and T. Lebey, "The effect of pulsed voltages on dielectric material properties," in IEEE Transactions on Dielectrics and Electrical Insulation, vol. 6, no. 1, pp. 20-26, Feb. 1999, doi: 10.1109/94.752005.

[5] M. Kaufhold et al "Failure mechanism of the inter-turn insulation of low voltage electric machines fed by pulse-controlled inverters," in IEEE Electrical Insulation Magazine, vol. 12, no. 5, pp. 9-16, Sept.-Oct. 1996, doi: 10.1109/57.537190.

[6] W. Yin "Failure mechanism of winding insulations in inverter-fed motors," in IEEE Electrical Insulation Magazine, vol. 13, no. 6, pp. 18-23, Nov.-Dec. 1997, doi: 10.1109/57.637150.

[7] W. Yin, K. Bultemeier, D. Barta, and D. Floryan, "Critical factors for early failure of magnet wires in inverted-fed motors," in Proc. IEEE Conference on Electrical Insulation and Dielectric Phenomena, San Francisco, CA Oct. 1995, pp. 258-261. doi: 10.1109/CEIDP.1995.483712

[8] G.C. Montanari, D. Fabiani, and A. Contin, "Ageing investigation of turn insulation under fast repetitive pulse voltage with or without partial discharges," in Proc. Coil Winding, Insulation and Electrical Manufacturing Exhibition, Berlin, Germany, June 1999, pp. 88-96.

[9] A. Cavallini et al "Power Electronics and Insulation Systems - Part 2: Life Modelling" 2010 IEEE Electrical Insulation Magazine 26-4.33-39.

[10] P. Wang, A. Cavallini and G. C. Montanari, "Characteristics of PD under square wave voltages and their influence on motor insulation endurance," in IEEE Transactions on Dielectrics and Electrical Insulation, vol. 22, no. 6, pp. 3079-3086, December 2015, doi: 10.1109/TDEI.2015.005158.

[11] P. Wang, A. Cavallini, G. C. Montanari and G. Wu, "Effect of rise time on PD pulse features under repetitive square wave voltages," in IEEE Transactions on Dielectrics and Electrical Insulation, vol. 20, no. 1, pp. 245-254, February 2013, doi: 10.1109/TDEI.2013.6451364.

[12] P. Wang, A. Cavallini and G. C. Montanari, "The influence of repetitive

square wave voltage parameters on enameled wire endurance," in IEEE Transactions on Dielectrics and Electrical Insulation, vol. 21, no. 3, pp. 1276-1284, June 2014, doi: 10.1109/TDEI.2014.6832275.

[13] P. Wang, A. Cavallini and G. C. Montanari, "The influence of square wave voltage duty cycle on PD behavior," 2015 IEEE Conference on Electrical Insulation and Dielectric Phenomena (CEIDP), Ann Arbor, MI, USA, 2015, pp. 338-341, doi: 10.1109/CEIDP.2015.7352006.

[14] T. Koltunowicz, A. Cavallini, D. Djairam, G. C. Montanari and J. Smit, "The influence of square voltage waveforms on transformer insulation break down voltage," 2011 Annual Report Conference on Electrical Insulation and Dielectric Phenomena, Cancun, Mexico, 2011, pp. 48-51, doi: 10.1109/CEIDP.2011.6232593.

[15] T. Koltunowicz, R. Kochetov, G. Bajracharya, D. Djairam and J. J. Smit, "Repetitive transient aging, the influence of repetition frequency," 2011 Electrical Insulation Conference (EIC)., Annapolis, MD, USA, 2011, pp. 444-448, doi: 10.1109/EIC.2011.5996195.

[16] D. Bortis et al "Design procedure for compact pulse transformers with rectangular pulse shape and fast rise times" in IEEE Transactions on Dielectrics and Electrical Insulation 18-1171, 2011.

[17] S. Candolfi et al "Hybrid design optimization of high voltage pulse transformers for Klystron modulators," in IEEE Transactions on Dielectrics and Electrical Insulation, vol. 22, no. 6, pp. 3617-3624, December 2015, doi: 10.1109/TDEI.2015.005047.

[18] D. Aguglia et al "Klystron modulator technology challenges for the Compact Linear Collider (CLIC)," 2011 IEEE Pulsed Power Conference, Chicago, IL, USA, 2011, pp. 1413-1421, doi: 10.1109/PPC.2011.6191626.

[19] E. H. W. M. Smulders et al "Pulsed power corona discharges for air pollution control," in IEEE Transactions on Plasma Science, vol. 26, no. 5, pp. 1476-1484, Oct. 1998, doi: 10.1109/27.736042.

[20] H. Akiyama et al "Industrial Applications of Pulsed Power Technology," in IEEE Transactions on Dielectrics and Electrical Insulation, vol. 14, no. 5, pp. 1051-1064, October 2007, doi: 10.1109/TDEI.2007.4339465.

[21] S. J. Beebe "Applications for Pulse Power using Nanosecond Pulsed Electric Fields (nsPEFs) in Cell Biology and Cancer Treatment" (2013). Bioelectrics Publications. 14.

[22] "Rotating electrical machines – Part 18-41: Partial discharge free electrical insulation systems (Type I) used in rotating electrical machines fed from voltage converters," IEC Standard 60034, 2014.

[23] R. Färber "Endurance of Polymeric Insulation under Mixed-Frequency Medium-Voltage Stress," PhD dissertation, ETH Zurich, 2019.

[24] P. K. Whitham "What is wrong with line-type modulators?" IECON'03. 29th Annual Conference of the IEEE Industrial Electronics Society (IEEE Cat. No.03CH37468), Roanoke, VA, USA, 2003, pp. 93-95 vol.1, doi: 10.1109/IECON.2003.1279961.

[25] W. J. Carey and J. R. Mayes, "Marx generator design and performance," Conference Record of the Twenty-Fifth International Power Modulator Symposium, 2002 and 2002 High-Voltage Workshop., Hollywood, CA, USA, 2002, pp. 625-628, doi: 10.1109/MODSYM.2002.1189556.

[26] R. Cassel, "The evolution of pulsed modulators from the Marx generator to the Solid State Marx modulator and beyond," 2012 IEEE International Power Modulator and High Voltage Conference (IPMHVC), San Diego, CA, USA, 2012, pp. 9-13, doi: 10.1109/IPMHVC.2012.6518666.

[27] S. M. et al., "Development of a Pulsed High Frequency Source for Testing Cellulosic Insulation Material for High Voltage Solid State Transformer Applications," 2018 IEEE International Conference on High Voltage Engineering and Application (ICHVE), Athens, Greece, 2018, pp. 1-4, doi: 10.1109/ICHVE.2018.8641793.

[28] K. Niayesh and E. Gockenbach, "On the aging mechanism of solid insulating materials exposed to repetitive high voltage pulses," in IEEE Transactions on Dielectrics and Electrical Insulation, vol. 21, no. 1, pp. 304-310, February 2014, doi: 10.1109/TDEI.2013.004055.

[29] "IEEE Standard for Pulse Transformers," IEEE Standard 390, 1987.

[30] G. N. Glasoe and W.H. Bostick "Pulse Generators" Chapter 14 Volume 5 MIT Radiation Laboratory Series, 1948.

[31] S. Stathis and J. Biela, "Optimal Design of a Transformer-based Solid-State Pulse Modulator with a Damping Network for Ultra-Fast Rise Times," 2021 23rd European Conference on Power Electronics and Applications (EPE'21 ECCE Europe), Ghent, Belgium, 2021, pp. P.1-P.11, doi: 10.23919/EPE21ECCEEurope50061.2021.9570450.

[32] M. Jaritz and J. Biela, "Isolation design of a 14.4kV, 100kHz transformer with a high isolation voltage (115kV)," 2016 IEEE International Power Modulator and High Voltage Conference (IPMHVC), San Francisco, CA, USA, 2016, pp. 73-78, doi: 10.1109/IPMHVC.2016.8012831.

[33] M. G. Niasar and W. Zhao "Aging of oil-impregnated paper at different frequencies," 2021 IEEE International Conference on the Properties and Applications of Dielectric Materials (ICPADM), Johor Bahru, Malaysia, 2021, pp. 430-433, doi: 10.1109/ICPADM49635.2021.9493911.

[34] B. Sonerud, T. Bengtsson, J. Blennow and S. M. Gubanski, "Dielectric heating in insulating materials subjected to voltage waveforms with high harmonic content," in IEEE Transactions on Dielectrics and Electrical Insulation, vol. 16, no. 4, pp. 926-933, August 2009, doi: 10.1109/TDEI.2009.5211835.

[35] A. Cavallini, E. Lindell, G. C. Montanari and M. Tozzi, "Inception of partial discharges under repetitive square voltages: Effect of voltage waveform and repetition rate on PDIV and RPDIV," 2010 Annual Report Conference on Electrical Insulation and Dielectric Phenomena, West Lafayette, IN, USA, 2010, pp. 1-4, doi: 10.1109/CEIDP.2010.5724033.

[36] J. P. Crine, "A molecular model to evaluate the impact of aging on space charges in polymer dielectrics," in IEEE Transactions on Dielectrics and Electrical Insulation, vol. 4, no. 5, pp. 487-495, Oct. 1997, doi: 10.1109/94.625641.

[37] H. R. Zeller, "Breakdown and Prebreakdown Phenomena in Solid Dielectrics," in IEEE Transactions on Electrical Insulation, vol. EI-22, no. 2, pp. 115-122, April 1987, doi: 10.1109/TEI.1987.298867.

[38] J. -P. Crine, "On the interpretation of some electrical aging and relaxation phenomena in solid dielectrics," in IEEE Transactions on Dielectrics and Electrical Insulation, vol. 12, no. 6, pp. 1089-1107, Dec. 2005, doi: 10.1109/TDEI.2005.1561789.

[39] P. Mathew and M. G. Niasar, "Lifetime of Oil-Impregnated Paper under Pulse Stress at Different Frequencies" Vol. 27 No. 1 (2022): Proceedings of the 27th Nordic Insulation Symposium (NordIS-22)

[40] P. Mathew "Pulsed Ageing of Oil-Paper: Test Modulators and Ageing Trends," MSc Thesis, TU Delft, 2021.

Philip Mathew was born in Mumbai, India in 1997. In 2019 he received a B.Tech. Electrical engineering from NIT-K Surathkal, India. At IIT-Delhi, he researched PV-based microgrids for spreading electricity access in rural areas. He received an M.Sc. Power engineering in 2021 from the TU Delft, The Netherlands; with a specialty in combining high-voltage physics and power electronics. His master thesis studied dielectric ageing phenomenon under high frequency pulsed stresses specifically seen in oil-paper insulations. During his studies, he also interned and later worked part-time in R&D for Prysmian Group. He is currently employed as an R&D engineer at Hitachi Energy in Ludvika, Sweden; working with BiMOS semiconductors in gigawatt HVDC converter systems. He will next join CERN in Geneva, Switzerland to design high-power electronics for their particle accelerators.

Mohamad Ghaffarian Niasar was born in Tehran, Iran, in 1984. He received the M.S. degree from the Sharif University of Technology, Tehran, in 2008, and the Ph.D. degree from the Royal Institute of Technology, Stockholm, Sweden, in 2015. He is currently an Assistant Professor at the High Voltage Technologies Group, Delft University of Technology, Delft, The Netherlands. His main research interests are the aging of electrical insulation, HVDC insulation, partial discharges, high-frequency power transformers, power cables, and FEM modeling.

Peter Vaessen (Member, IEEE) was born in Maasbree, The Netherlands, in 1960. He received the M.Sc. degree (cum laude) in electrical power engineering from Eindhoven Technical University, The Netherlands. In 1985, he joined KEMA (now a CESI brand). In his 35-year career, he held research positions in the field of large power transformers and high voltage measurement and testing. He has 25 years of experience in (U)HVDC technology and T&D grids with high shares of renewables. He is manager innovations with KEMA Laboratories and Chairman of the European Distributed Energy Resources Laboratories association (DERlab). Since 2017, he has been a Part-Time Professor of Hybrid Transmission Systems with the Delft University of Technology, where he teaches courses on both high voltage technologies and HVDC.